T.2: Growth, characterization and application of $LiNbO_3$ and $Li_2B_4O_7$ single crystals

K. S. Bartwal
Laser Materials Development & Devices Division
bartwal@rrcat.gov.in

We have intense program to prepare single crystals for nonlinear optical applications apart from the strengthening of the basic understanding of crystal growth mechanism. These crystals have many applications e.g. harmonic generation of laser light, E-O modulator, Q-switch, etc. Some of these crystals are of great interest because of their most favorable electro-optic, acousto-optic, ferroelectric and photorefractive properties. There are several techniques to grow single crystals. In this article, I will confined to the crystals grown by melt technique particularly the Czochralski growth. The crystals to be taken up in this article are: $LiNbO_3$, $Li_2B_4O_7$ and their doped variants. The structure of the crystal gets modified on doping with desired transition metal ion which intern change the crystal properties. The structural and optical characterization of grown crystals were carried out using powder XRD, TEM, optical microscopy, spectrophotometer etc. The possible applications of these crystals will be highlighted. Crystal growth is difficult, expensive and time taking process. Recently, we have planned to explore the possibility of developing nanocrystalline variants of these materials in a suitable matrix with the aim to replace single crystals.

1. Introduction:

A material having 3-dimentional periodic arrangement of atoms/molecules extending up to infinity is called crystal. Man had admired crystals for long, as he had appreciated beauty. The gems and crystals delivered by mother earth have always attracted our mankind, and the belief in the virtues of gems and some minerals dates back to at least two thousand years. Today, crystals are pillars of modern electronic and optical technologies and devices. Progress in crystal growth and epitaxy technology is highly demanded in view of its essential role for the development of several important optical areas such as solid state lasers, bright long-lifetime LEDs, waveguides, nonlinear devices, high-efficiency photovoltaic cells and detectors for variety of applications like communications, alternative energy, medicine and materials processing. Integrated microelectronic and optoelectronics necessitates improved growth technology for large diameter Si, Ge, GaAs, InP, $LiNbO_3$, $Li_2B_4O_7$, PbB_4O_7 and $LiTaO_3$. Growth of crystal ranges from a small inexpensive technique to a complex sophisticated expensive process, and the crystallization time ranges from minutes, hours, days, months and to several years.

$LiNbO_3$ single crystals show large nonlinear optical, piezoelectric, pyroelectric, electro-optic and acousto-optical coefficients. It also show photo-elastic, photorefractive, acousto-optic and birefringent effect. Near stoichiometric LN crystal is transparent for the wavelengths between 350 and 5200 nm and has a band gap around 3.9 eV. Due to these excellent properties, LN single crystal is of great interest since several decades for both fundamental sciences and applications in optics such as second harmonic generators, optical amplitude modulators, Q-switches, beam deflectors phase conjugators, dielectric waveguides, holographic data processing device, memory element, SAW devices etc.

The NLO crystals based on B-O bond (borate family) are promising because of transparency in deep UV region (wide band gap), high damage threshold and high non-linear coefficients. This is due to the large difference in electro-negativities of B and O atom on the B-O bond. The crystals based on borate rings exist in numerous structural types, and crystals like BaB_2O_4, $Li_2B_4O_7$, PbB_4O_7 and $CsLiB_3O_5$ are excellent non-linear optical materials, particularly in the ultraviolet region. Lithium tetraborate, $Li_2B_4O_7$ (LTB) is promising materials in this series with its specific features like non-hygroscopic, high mechanical and optical strength, transparency in deep UV region. The congruent melting makes the crystal growth simple and therefore, high optical quality crystals can be grown. $Li_2B_4O_7$ due to its UV transparency is an important material for generation of 4th and 5th harmonic generation of Nd: YAG laser and frequency conversion devices for high power UV solid-state laser.

Once the crystals are grown, it is must to characterize them for crystalline perfection and optical homogeneity before putting them to device applications. This article aim to highlight the crystal growth of some of the important NLO materials and their thorough structural and optical characterization, so that they qualify the commercial standards for device application.

2. Crystal growth:

Crystal growth is involved with the control of a phase change. It is basically an isothermic, isobaric, reversible process. On the basis of this, crystal growth may be classified into three categories as follows:

Solid Growth - Solid to Solid phase transformation
Liquid Growth - Liquid to Solid phase transformation
Vapour Growth - Vapour to Solid phase transformation

In this article, I will cover only few materials (e.g. $LiNbO_3$, $Li_2B_4O_7$) which are grown by Czochralski crystal pulling technique. The main idea of the Czochralski process was developed in the year 1918 by polish scientist Jan Czochralski (1885-1953). Czochralski (Cz) pulling is the process of crystal growth in which the material is melted in a suitable crucible and a rotating seed crystal is dipped into the melt and slowly withdrawn. During this withdrawal process the crystal grows on the seed. In Cz technique, growth can be achieved in controlled manner and in any crystallographic direction with oriented seed. The Czochralski crystal puller was designed and fabricated at RRCAT and was used for growing these crystals. Fig.T.2.1 shows the schematic of the growth chamber and the Cz crystal puller developed in the laboratory.

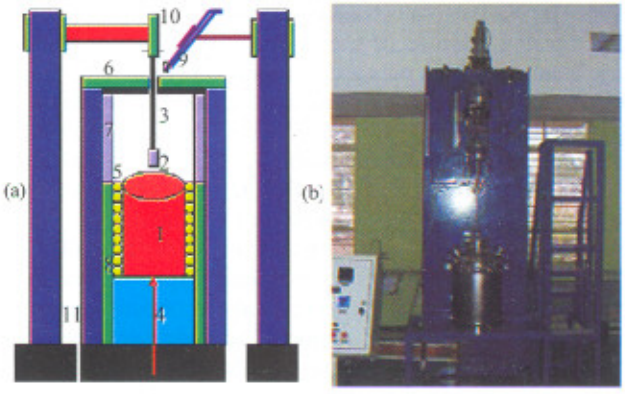

Fig.T.2.1 : Schematic of growth chamber and Crystal Puller developed at RRCAT

3. Lithium Niobate:

Lithium niobate, $LiNbO_3$ (LN) is technologically important material because of its favorable electro-optic, acousto-optic, ferroelectric and photorefractive properties [1-4]. It has distorted perovskite (ABO_3) unit cell with 3m point group symmetry and R3c space group in the trigonal (rhombohedral) phase at room temperature. The lattice parameters of the trigonal unit cell are a = 5.4944Å, α = 55°87". Sometimes, it is more convenient to choose a hexagonal unit cell for $LiNbO_3$ with lattice parameters a_H = 5.1483 Å, c_H = 13.8631Å. $LiNbO_3$ is a typical non-stoichiometric material. It always grow at congruent melt composition of 48.6 mol% Li_2O and 51.4 mol % Nb_2O_5 and is known as congruent lithium niobate (CLN). The binary phase diagram of Li_2O-Nb_2O_5 system is shown in Fig.T.2.2. From the phase diagram, it can be seen that the congruent composition is at 48.6 mol% of Li_2O. Crystals grown from melt compositions other than congruent show composition variations along the crystal length affecting several physical properties. The Li-deficiency in LN crystals, lead to high concentration of intrinsic defects (vacancies, anti-site defects etc.) and high disorder. The defect site can cause absorption and incorporation of impurities. The presence of these defects and impurities makes LN low damage resistant to optical radiation.

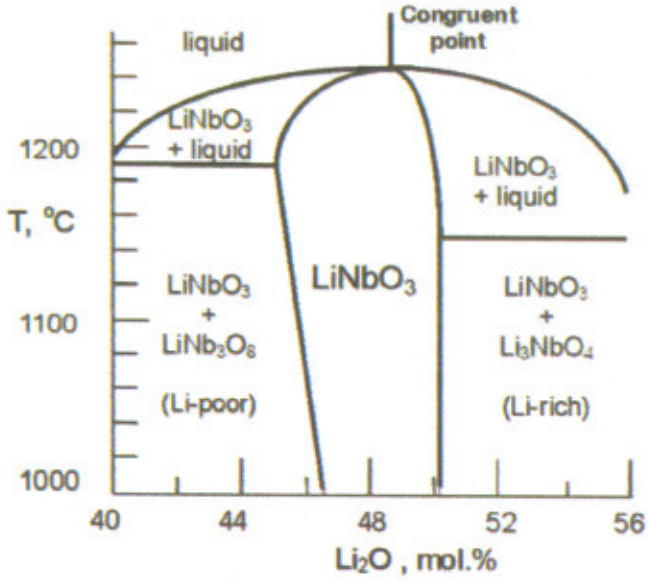

Fig.T.2.2 : Phase diagram of Li_2O-Nb_2O_5 system

High concentration of intrinsic defects causes vacancies V_{Li}, anti-site Nb_{Li} and polarons formation in the CLN. The well understood vacancy model for CLN are:

Li site vacancy model:

$$[Li_{1-5x}Nb_xV_{4x}][Nb][O_3]$$

Nb site vacancy model:

$$[Li_{1-5x}Nb_{5x}][Nb_{1-4x}V_{4x}][O_3]$$

These vacancies in CLN results into low damage resistant to optical radiation, absorption and incorporation of impurities, high switching field, decline in EO, NLO properties. On the other hand, stoichiometric lithium niobate (SLN) has enhancement in NLO and EO properties, high damage threshold, transparent to shorter wavelengths,

less intrinsic defects, low scattering losses, low domain switching field. The unit cell of LN crystal and the possible vacancy site are shown in Fig.T.2.3.

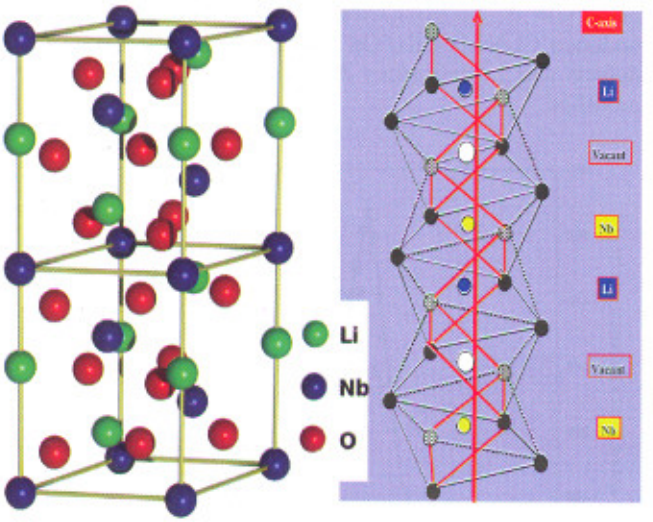

Fig.T.2.3 : The hexagonal unit cell of LN crystal with the vacancy site

The physical properties of $LiNbO_3$ crystal changes with change in Li/Nb ratio. These intrinsic defects in the form of Li deficiency are compensated by added extrinsic defects such as Mg, Zn, Sc, In, ion doping to make the material damage resistant to optical radiation. One of the most studied dopant in $LiNbO_3$ is Cr^{3+} ion. Several Cr^{3+} centers have been detected in $LiNbO_3$ crystals [5-7]. There are differences in the bond length for the Li-O and Nb-O octahedrons and there is a large lattice relaxation that occurs when doped with Cr^{3+} ions. LN doped with transition metal ions such as Cu, Fe, Mn, Zn etc., exhibit significant photorefractive property and is potential material for holographic memories [8]. Recent studies have shown that Fe:LN crystals have good potential for high-density data storage applications. Both, photorefractivity and quality of holography depends on the presence of defects generated by growth conditions as well as deliberately doped transition metal ions. It is also reported that Fe doped LN can be used as pyroelectric infrared sensor [9-12]. It has also been reported that in Cr:LN and Nd:LN the addition of Mg^{2+} leads to appearance of additional OH^- infrared absorption bands which arises due to formation of Cr^{3+}- OH^--Mg^{2+} and Nd^{3+}-OH^--Mg^{2+} centers, respectively [13-15]. The OH^- ions are always present in air grown $LiNbO_3$ crystals. The infrared absorption band at about 3487 cm^{-1} is caused by the stretching vibration of OH^- dipoles in pure LN crystal. In Mg:LN crystal the OH^- stretching vibration frequency increases from 3487 to 3535 cm^{-1}.

$LiNbO_3$ single crystals were grown in air atmosphere by Czochralski technique from a congruently melting composition [16]. As has been mentioned above, LN is known to have a fairly large solid solution range from 42 to 52 mol% Li_2O. The melting point for the congruent composition (48.6 mol% Li_2O and 51.4 mol% Nb_2O_5) is 1250 ± 5 °C. The platinum crucible was used for crystal growth. The [001] oriented seed of dimension 2.5x2.5x20 mm^3 was used for growth. Pulling rate was in the range 2-4 mm/h in the body part of the boule and the rotation rate was kept at 12-25 rpm. The post growth cooling was maintained at 20-30 °C/h initially up to 1000 °C and thereafter fast cooling to room temperature. The growth parameters were optimized for undoped and doped variants of LN. Good optical quality crystals were grown. Fig.T.2.4 shows some of the as grown crystal boules and the cut and polished crystal elements of undoped and doped LN crystals. The doped crystals: 3, 5 and 7mol% Mg, 0.1, 0.25 and 0.5 mol % of Cr, 0.03 mol% Fe were grown successfully. The Mg, Cr, co-doped LN (7mol% Mg and 0.5 mol% Cr) single crystals were also grown. Distribution coefficient of Mg is 1.2, Mn is 1.0 and Fe is 0.92 in $LiNbO_3$ irrespective of doping concentration.

Fig.T.2.4 : The as grown crystal boules and elements of undoped and doped $LiNbO_3$

Specimens from the crystal boule were cut along the various crystallographic directions (see Fig.T.2.4). All the Specimens were lapped and polished with fine alumina powder. The thicknesses of the polished samples were taken ~1 mm. These polished crystal wafers were used for characterization purposes. These crystal elements were characterised for their phase and crystallinity using powder XRD, high resolution XRD and transmission electron microscopy. A small portion of the grown crystal was crushed and the crystalline powder was analyzed by XRD. Fig.T.2.5

shows the representative powder XRD pattern for undoped congruent composition LN crystal. Similarly, powder XRD were taken for doped crystals as well. The dopant concentration is very small and there is no change in basic structure of LN, therefore, we could not see any difference between the XRD patterns for undoped and doped samples. The modification in structure is observed at microscopic level. The presence of doped ion could be investigated by other indirect means.

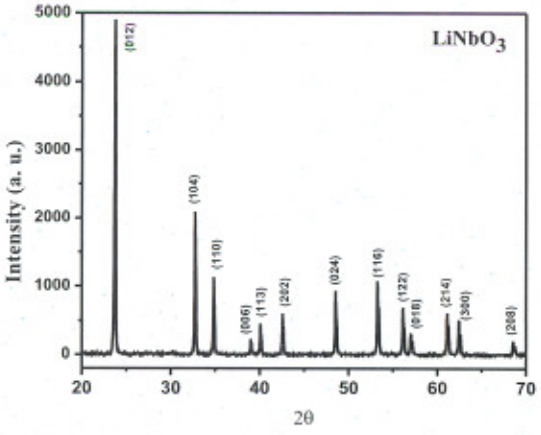

Fig.T.2.5 : Powder XRD pattern for as grown undoped congruent

To study the crystalline perfection, high-resolution X-ray diffractometry and X-ray topography is best tool [17, 18]. A well-collimated Mo $K\alpha_1$ beam diffracted from a set of three plane monochromator crystals of Si (111) in the dispersive symmetrical Bragg geometry (+, -, -) configuration. This arrangement improve the spectral purity of the $K\alpha_1$ beam. The specimen crystal was aligned in the (+, -, -, +) symmetrical Bragg geometry. The specimen can be rotated in steps of 0.5". The diffracted X-ray intensity is measured by a scintillation counter. The output is measured by the counting system incorporated in the microprocessor control unit. The detector is mounted with its axis along a radial arm of the turntable. Fig.T.2.6 shows the high resolution X-ray diffraction curves (DC) for undoped and Mg, Nd co-doped $LiNbO_3$ crystal. From the DC it is clear that it contains one extra peak along with main peak corresponding due to low angle (≥1 arc min) grain boundary. The additional peak is at 95 arc sec towards higher diffraction angle from the main peak. The full-width at half maximum (FWHM) of the main peak is 20 arc sec, while the peak intensity was measured 550 c/sec. The additional peak in the observed DC cannot be due to the ferroelectric domain boundaries. DC in Fig.T.2.6 (b) clearly shows that there is only single peak in Mg, Nd co-doped crystal. The half width and peak intensity of this peak are 19 arc sec and 1145 c/sec, respectively. Nearly full height of the DC, which is approximately equal to the height of the exploring X-ray beam reveals that the specimen does not contain any structural boundaries. This DC indicate that crystalline perfection of Nd:Mg:$LiNbO_3$ is much better compared to undoped CLN crystals. On Nd:Mg doping the Nd anti-site defects and Li deficiency decreases and the structure gets modified.

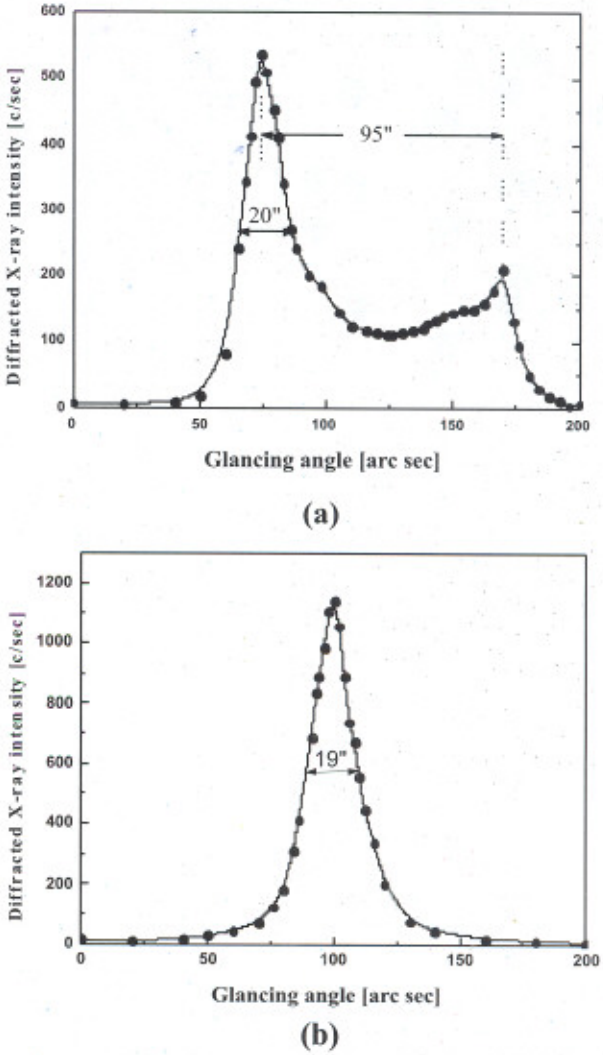

Fig. T.2.6 : High resolution X-ray diffraction curve recorded for (006) diffracting planes of (a) undoped (b) Mg, Nd co-doped $LiNbO_3$ crystals [17]

Fig.T.2.7 shows the DC and topographs for (006) diffracting planes of the Fe-doped LN single crystal for as-grown (A), annealed at 973 K (B) and annealed at 1323 K (C). The inset in the Fig.T.2.7, (a) - (f) are the section topographs recorded at the peak positions. The well- resolved multiple peaks are

indicative of structural grain boundaries in the as grown crystals. Also there are crystalline defects present in the Fe doped crystals. On annealing at high temperature, some of the crystalline defects get annealed out. The deconvolution of this curve indicates that the experimental DC consists of two curves (dotted lines) with an angular separation of 10 arc sec. After further annealing at 1323 K, the very low-angle boundary at 10 arc sec has also been removed, as in Fig.T.2.7(C). The asymmetric shape of the diffraction curve in Fig.T.2.7C indicates that the specimen contains quite a large number of vacancies and their agglomerates, which give rise to Bragg diffraction intensities at lower diffraction angles and lead to asymmetry and broadening of the DC.

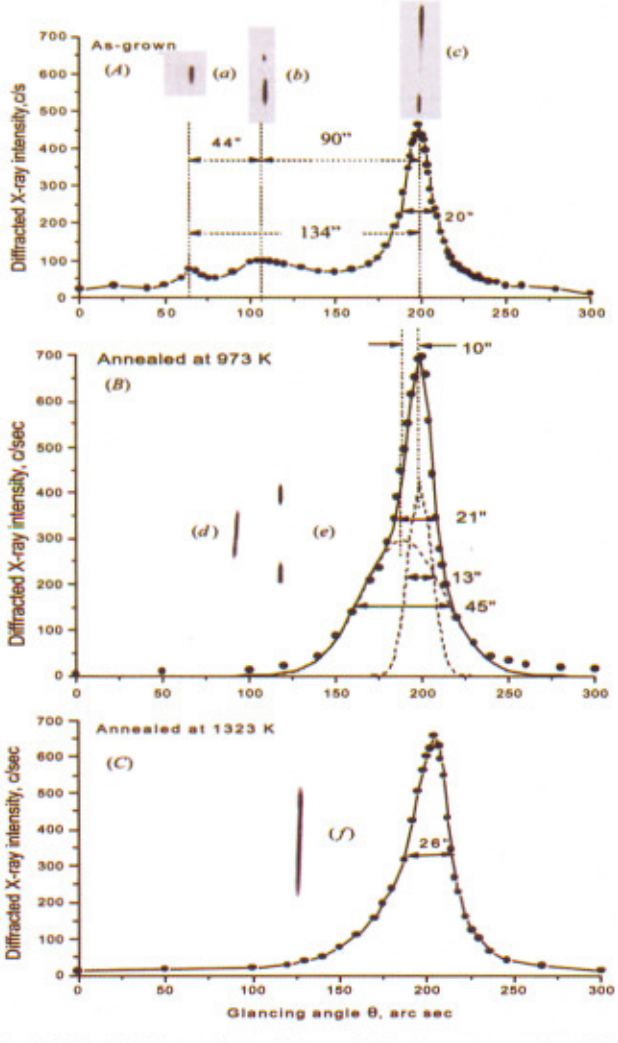

Fig.T.2.7 : High resolution X-ray diffraction curves for (006) diffracting planes of the Fe-doped $LiNbO_3$ single crystal: (A) as-grown, (B) annealed at 973 K and (C)) annealed at 1323 K. The insets (a) – (f) are the section topographs recorded at the peak positions [18]

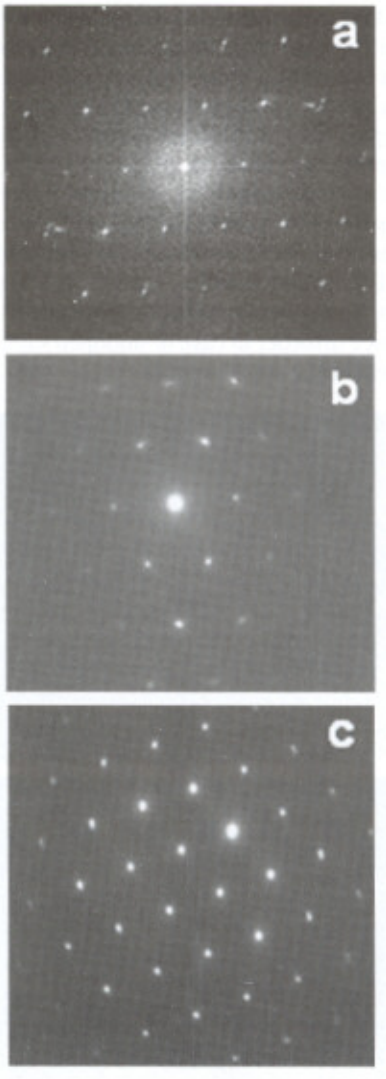

Fig.T.2.8 : SAED patterns for undoped, 1 mol% and 3 mol% Mg doped $LiNbO_3$ crystals. The lattice disorder reflected in terms of streaks connecting diffraction spots is clearly seen

Transmission electron microcopy (TEM) is useful tool to know about the local structure of the material [19, 20]. The phase, crystallinity, crystallite sizes and microstructure were investigated using transmission electron microscopy (TEM) in diffraction and high-resolution mode. Philips make, Technai G^2-20 (FEI) electron microscope operating at 200 kV was used for TEM experiments. Sample for TEM observation was prepared by suspending the particles in ethanol by ultrasonification and drying a drop of the suspension on a carbon coated copper grid. Fig.T.2.8 shows the selected area electron diffraction (SAED) patterns for undoped, 1 mol% and 3 mol% Mg doped $LiNbO_3$ crystals. The SAED pattern (Fig.T.2.8a) is clearly

indicating that in undoped LN samples the intrinsic defects arises from Li deficiency, are responsible for the diffuseness and streaks connecting spots. In Fig.T.2.8b, the diffuseness is reduced as the Li vacancies are decreased in 1 mol% Mg doped samples. The defect level is much less in 3 mol% Mg doped samples as seen in Fig.T.2.8c, the streaks and diffuseness is almost absent. Similar results are expected from HRTEM images taken from undoped and 3 mol% Mg doped LN samples. The HRTEM images for undoped and 3 mol% Mg doped LN are shown in Fig.T.2.9 (a, b). As can be seen in Fig.T.2.9 (a, b), the crystalline defects are clearly visible in the form of lattice disorder in case of undoped sample, which are almost absent in Mg doped sample.

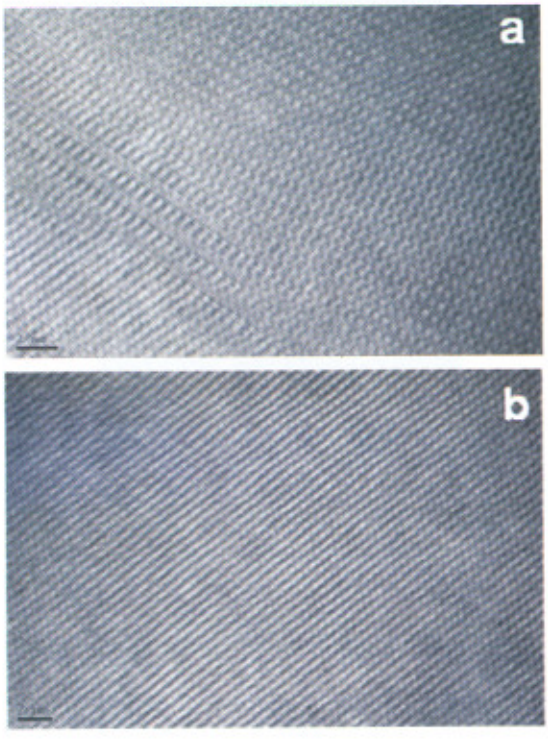

Fig.T.2.9 : HRTEM micrographs for undoped and 3 mol% Mg doped $LiNbO_3$ crystals. The lattice disorder reflected in terms of missing planes is clearly seen

The optical homogeneity of the grown crystal is very crucial for its device application. The Li/Nb ratio is governing factor in optical parameters as well. The physical properties sensitive to Li/Nb ratio are: extraordinary index of refraction, transparency in UV, absorption edge (UV), phase matching temperature (T_m), Curie temperature (T_c) and Raman scattering. The relation between UV absorption edge and Li_2O content:

$$y = -247.4663 + 1.9888\,x - 0.00332\,x^2$$

where, x is UV absorption edge and y is Li_2O content (mol.%). For optical homogeneity, the transmission, birefringence and conoscopy investigations are necessary.

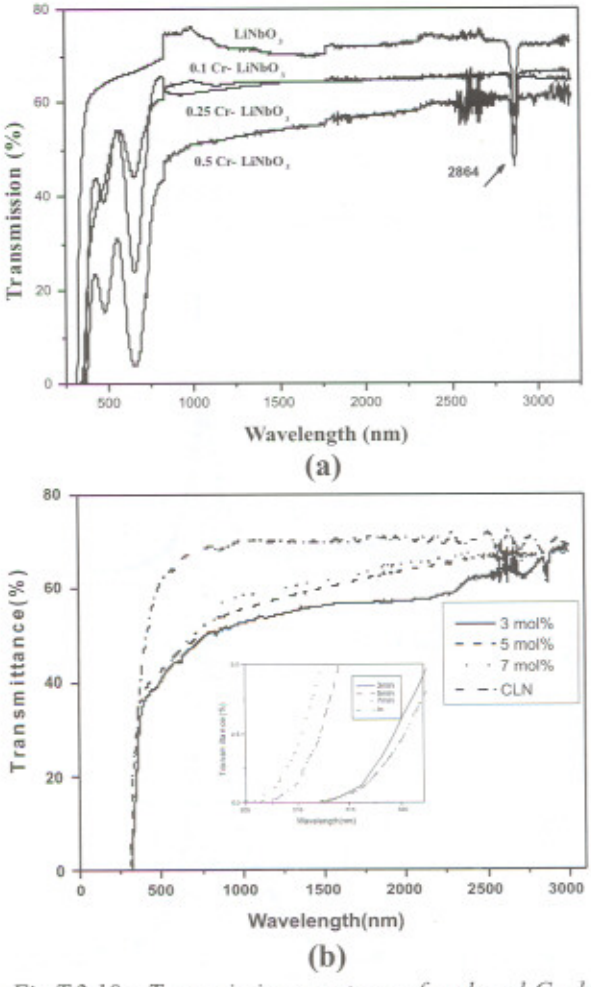

Fig.T.2.10 : Transmission spectrum of undoped Cr doped and Mg doped $LiNbO_3$ crystal slices. Undoped crystal shows about 75% transmittance

Optical transmission spectra of doped and undoped samples were recorded for wavelength ranging 300-3200 nm using Shimadzu UV 3101PC spectrophotometer. Fig.T.2.10 (a, b) shows the representative transmission spectra for undoped, Cr doped and Mg doped LN crystals. It is clear from the Fig.T.2.10a, that UV cutoff wavelength increases (red shift) in Cr- doped samples which indicates the overall decrease in Li/Nb ratio [21]. The octahedral crystal field around the Cr^{+3} ion splits the ^4F level into a ground state orbital singlet $^4A_2$ and excited state orbital triplets $^4T_2$ and $^4T_1$. Also due to the crystal field, splitting of the free ion excited state ^2G gives

rise to level ^{2}E. On the other hand, Fig.T.2.10b, clearly show that in Mg doped LN, the blue shift is present. It is due the increase in Li/Nb ratio i.e. the defect concentration reduces in the crystal. The blue shift increases with increasing Mg doping concentration. The broad symmetrical OH bond stretching absorption band is observed at 2864 nm.

Optical conoscopy pictures were taken from thin polished crystal plates (z-cut, 0.5 mm thick). Fig.T.2.11 shows the representative conoscopy patterns taken for an undoped, Fe-Mn co-doped LN crystals. The sharpness of the fringes and the uniform intensity distribution confirms that there is practically none or very little strain in the grown crystals. This further establishes the good optical quality of the grown crystals.

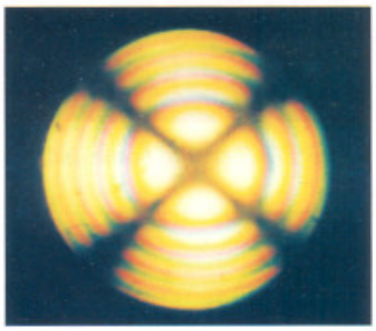

(a)

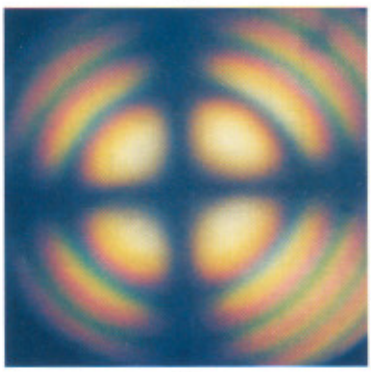

(b)

Fig.T.2.11 : Conoscopy patterns for (a) undoped and (b) Fe-Mn co-doped $LiNbO_3$

The optical homogeneity of the crystal was also measured using birefringence interferometry technique. Fig.T.2.12 shows the representative birefringence interferogram for doubly doped Fe:Mn-LN crystal. The straight and equispaced fringes indicate that the crystal has uniform dislocation density and good refractive index homogeneity. This confirms that the grown crystal is of good optical quality. The birefringence along the *a*-axis was computed as:

$$\Delta n = n_e - n_o = (\lambda N / L)$$

where λ, N, and L are wavelength of laser used, number of fringes in the interferogram and thickness of the sample. Using, λ = 632.8 nm, N = 8 and L = 1.1 mm, we get the birefringence of the Fe:Mn-$LiNbO_3$ crystal along a- axis as 0.004602 [22, 23].

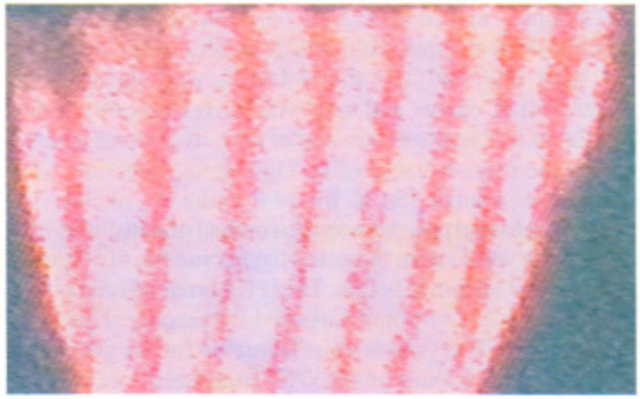

Fig.T.2.12 : Birefringence interferogram of a Fe-Mn $LiNbO_3$ crystal along a-axis

4. Lithium Tetraborate:

Lithium tetraborate, $Li_2B_4O_7$ (LTB) is an important material for generation of 4th and 5th harmonics of Nd: YAG laser and frequency conversion devices for high power UV solid-state laser. LTB belongs to tetragonal crystal system having 4mm point group symmetry with lattice parameters, a = b = 9.479 Å, c = 10.286 Å. High electromechanical coupling coefficient factor k^2 and low temperature coefficient of frequency has made LTB crystal very attractive material for surface acoustic wave substrate. Microwave devices using surface acoustic waves are in common use for infrared filters for color television and signal processing elements. Transmission range of this crystal is 170 nm – 3300 nm. The damage threshold value of ~10 GW/cm^2 for LTB crystal is the largest among the borate crystal. Lithium triborate (LBO) and cesium triborate CLBO) both have vanishing effective non-linearity in the limit of 90° non-critical phase matching. But effective non-linearity is maximum for LTB crystal under 90° phase matching. LTB is also considered to be one of the useful materials for neutron detection because it contains Li and B, which possess large neutron capture cross-section. This material has attracted much attention for application in radiation dosimetry. Tissue equivalence is a much desired property for thermoluminescent dosimeters for estimation of absorbed dose in the tissues. Over gamma-ray energy region

(20-100 keV) the photoelectric interaction is predominant and depends on the third power of the atomic number (Z). Therefore, the atomic number of a dosimetric material should match as close as possible to that of the biological tissue. LTB based TL dosimeters are best with an effective atomic number of 7.3 which is very close to that of soft biological tissue (Z_{eff}=7.42).

Undoped and doped LTB crystals were grown by Czochralski technique. High purity oxides in the ratio 67.9 mol % of B_2O_3 and 32.1 mol% Li_2CO_3 were taken for the preparation of charge and they were mixed properly in ball mill for 24 h. The excess amount of B_2O_3 over stoichiometric composition was because of its high vapour pressure. The mixture was kept at 350 °C for 24 h in the Pt crucible. The solid state reacted powder was then melted directly at 917 °C. The growth was carried out using the Pt crucible of 50 mm in diameter and 50 mm in height. The [110] oriented seed crystal of dimension 2×2×10 mm^3 was used for seeding. This [110] direction in LTB crystal is most favorable for the generation of 4th and 5th harmonics of Nd:YAG laser. Seed was properly tied in ceramic rod with platinum wire and slowly dipped into the melt to avoid thermal shock. Initial rotation rate of the seed rod was kept 8 rpm and then reduced to 6 rpm afterward. Small rotation rate reduces thermal convection and hence reduces temperature fluctuations. Pulling rate was kept at ~0.2 mm/h. The cracking is a big problem with this crystal. Crystal generally cracks during post growth cooling due to anisotropy of thermal expansion coefficient. Grown crystals were cooled slowly in 24 h to room temperature to avoid the thermal shock. The temperature gradient along growth axis plays key role in minimizing the cracks. The crystals were grown with different temperature gradient and finally optimized the temperature [24]. The axial temperature gradient was optimized at 16 °C/ cm above the melt level, and 10 °C/ cm below the melt level. In this condition, a good quality and crack free crystals with facets were grown.

Fig.T.2.13 shows the grown crystal boule and processed elements. The grown crystals were cut into wafers for transmission studies. Crystal plates of dimension 10×10×1mm^3 were polished with 0.05-micron size alumina powder. The transmission of the crystal was observed more than 80 % over its transparent spectral range. The crystals were characterized for phase identification using X-ray powder diffraction. The optical homogeneity was investigated using transmittance measurements [25-27].

The crystalline phase of the grown crystals was determined by powder X-ray diffraction. The energy dispersive analysis of X-rays (EDAX) technique was used to confirm the doping concentration in the grown crystals.

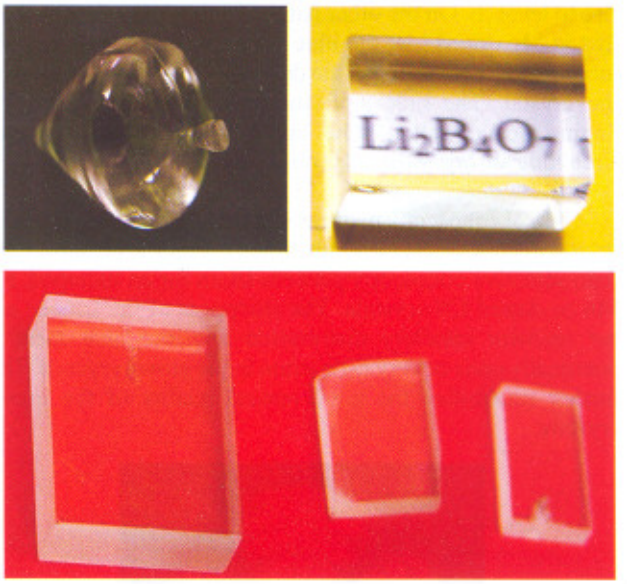

Fig.T.2.13 : LTB crystal boule and elements

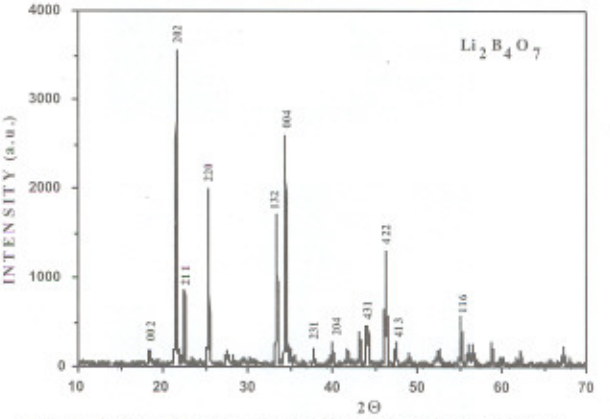

Fig.T.2.14 : XRD pattern of undoped LTB crystal

Fig.T.2.14 shows the representative powder XRD pattern for undoped LTB crystal. The XRD results confirm the growth of parent phase of $Li_2B_4O_7$. The doping of small amount does not reflect in the XRD results, however, EDAX confirms their doping into the crystal lattice.

The $Li_2B_4O_7$ single crystals doped with 1 mol% Mn were grown specifically to investigate the thermoluminescence properties. These samples were irradiated with different dose using Co-60 gamma source. Transmittance spectra of the crystal wafer irradiated with different gamma dose were recorded using UV-Vis spectrophotometer (Cary-50). Fig.T.2.15 shows the transmittance of before and after γ-irradiated LTB crystal samples. Several absorption peaks were observed in the transmission spectra. Main peaks are

observed at 366 nm, 471 nm and 594 nm. It has also been observed that the cutoff wavelength and the depth of the absorption peak increases with increasing dose. These absorption peaks corresponds to the respective crystalline defect levels generated during the irradiation. The concentration of these defect levels increases with higher dose, resulting in more electrons to trap and hence the increase in the depth of the absorption peak. The overall transmittance becomes low in the irradiated samples due to increased defect density.

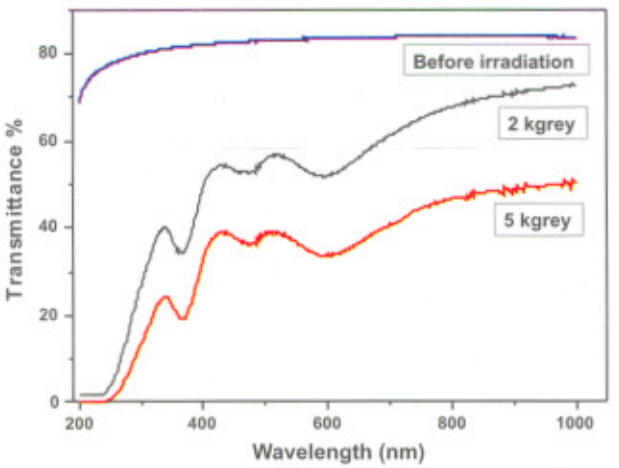

Fig.T.2.15 : Transmission spectra of Mn: LTB before and after γ-irradiation

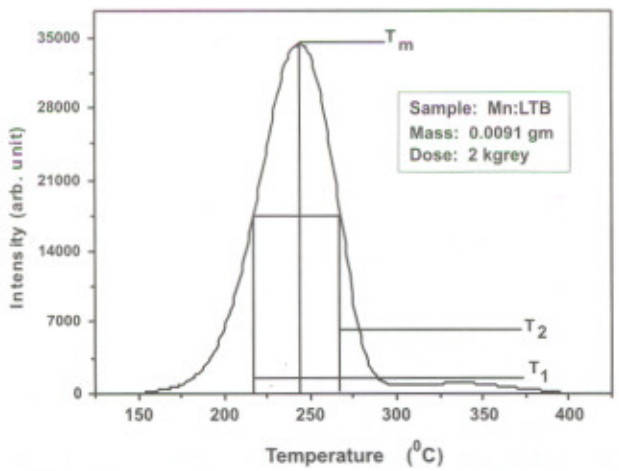

Fig.T.2.16 : Thermoluminescence spectrum of Mn:LTB

The TL spectrum of γ-irradiated Mn-doped LTB is shown in Fig.T.2.16. TL spectrum was taken by TLD reader analyzer (model- RA04). For an ideal crystalline semiconductor or insulator Z(E) = 0 when $E_c > E > E_v$. Here E_c is the bottom of the conduction band and E_v is the top of the valance band. However, when the structural defects occurs in crystal, or if there is impurities within the crystal lattice, there is a breakdown in the periodicity of the crystalline structure and it become possible for the electrons to posses energies which are forbidden in the perfect crystal. Whenever we heat the sample the trapped electrons go to the conduction band and recombine with hole available. The luminescence occurs during this process. The order of kinetics is also determined from the glow curve from the shape of the curve. First-order luminescence peak is asymmetric in nature with most of the peak area being on the low temperature side of the maximum at T_m. The second order luminescence peak is more symmetric in nature. Fig.T.2.16 also shows that the order of kinetics of the glow curve is "First- Order". The area under dosimetry peaks is direct measure of the amount of Mn^{2+} ions.

5. Summary, Potential Applications and Future Scope:

To summaries, single crystals of $LiNbO_3$, and $Li_2B_4O_7$ were grown successfully using high temperature melt (Czochralski) technique. The doped variants of these materials were also grown with the aim to investigate their specific properties and effect on the desirable characteristics. The growth parameters and doping concentration were optimized in each case separately. The role of the dopant ion(s) has been investigated in terms of modifications in the microstructure and consequently the physical properties. In case of $LiNbO_3$ crystals, it was found that the structure get modified on doping of various transition metal ions. The present investigations shows that the structure modification by doping enhances several physical and optical properties of $LiNbO_3$ crystal. These doped variants can be used for several optical, electro-optical and photo refractive applications. $Li_2B_4O_7$ crystals are of great interest in 4th and 5th harmonics of Nd:YAG laser. High laser damage threshold value of the order of ~8-10 GW/cm^2 was observed in the grown crystals. The Mn doped LTB is potential candidate for low dose human dosimetry application.

The potential applications of undoped and doped LN are numerous. The SAW device of LN; e.g. high sound velocity in this crystal, make it the best crystal as delay line in CTV. All CTV and mobile phone have at least one delay line made of LN crystal element. On doping of Ti, Ni, Cu, enhances further SAW velocity in LN which is used for phase conjugate wave generator. The LN crystal is birefringent, negative uniaxial with Δn = -0.08 and transparency range, 0.4 - 5.5 μm, makes it good choice for linear EO modulator, travelling wave modulator, wave guide modulator, and electro-optic Q-switches. The nonlinear devices e.g. SHG, optical parametric oscillator, quasi phase matching by making

alternating laminar domain structure are also being made using LN crystals. Photorefractive devices e.g. read /write hologram devices are being made using Fe doped LN crystals. Lithium tetraborate is promising materials in the borate series due to favorable characteristics like non-hygroscopic, high mechanical and optical strength, deep transparent in UV region. High electromechanical coupling coefficient factor k^2 and low temperature coefficient of frequency of LTB crystal has made it an attractive material for SAW substrate. LTB has effective atomic number of 7.3 which is very close to that of soft biological tissue (Z_{eff} = 7.42), which makes this material best choice for low level human dosimetery.

As has been described above, crystal growth is an expensive and time taking process. To exploit our experience on materials characteristics of $LiNbO_3$ and $Li_2B_4O_7$, we explored the possibility of preparation of the nanoparticles of these materials. These nanoparticles could be dispersed in suitable glass/polymer matrix. The elements made of these nanoparticle dispersed glass/polymer matrix, can possibly replace the crystal elements. In LN, it has been reported that the NLO properties changes when the particle sizes are below 50 nm. The SHG intensity of LN nanoparticles has been reported to enhance by an order of magnitude. Many synthesis routes are being followed for nano materials, e.g. ball milling, non-aqueous route, sol-gel method or hydrothermal route. We have initiated the preparation of LN and LTB nanoparticles by modified sol-gel and ball milling techniques. We have achieved the particle sizes below 50 nm. In the process of the search for suitable matrix, we have explored the possibility of using glass and PMMA. Some initial encouraging results have been found, those will be reported elsewhere.

Acknowledgement:

The author would like to thank his colleagues and collaborators who have contributed at different stages. Specially Shri Sujan Kar, R. K. Choubey, Namita Sisodia, Pratima Sen, Rajeev Bhatt, Sunil Verma have contributed significantly. The author would like to thank Dr. P.K. Gupta, Head, LMDDD for his interest and constant support.

References:

[1] A. Rauber, in: E. Kaldis (Ed.), Current Topics in Materials Science, Vol. 1, North-Holland, Amsterdam, 1978, p. 481.

[2] G. I. Stegeman, R. Schiek, Y. Back, *J. Opt. Soc. Am.* B **15** (1998) 2255-2268.

[3] H. F. Taylor, O. Eknoyan, *Appl. Opt.* **39** (2000) 124-128.

[4] I.V. Kityk, M.M. Janusik, M.D. Fontana, M. Allerie, F. Abdi, Cryst. Res. Technol. **36** (2001) 577-588.

[5] G. Malovichko, V. Grachev, E. Kokanyan, O. Schirmer, Phys. Rev. B **59** (1999) 9113-9125.

[6] R.K. Choubey, P. Sen, S. Kar, G. Bhagavannarayana, K.S. Bartwal, Solid State Commun. **140** (2006) 120-124.

[7] S. Kar, H. Ryu, K.S. Bartwal, The Open Crystallography Journal, **1** (2008) 1-5.

[8] T. Tsuboi, M. Grinberg, S.M. Kaczmarek, J. Alloys & Compounds, **341 (2002)** 333-337.

[9] T. Gebre, A.K Batra, P. Guggilla, M.D. Aggarwal, R.B. Lal, Ferroelectric Lett. **31 (2004)** 131-139.

[10] S. Kar, S. Verma, K.S Bartwal, Crystal Growth and Design, **8** (2008) 4424–4427.

[11] S. Kar, Sunil Verma, M.W. Shaikh, K. S. Bartwal, Physica B **404** (2009) 3507-3509.

[12] S. Kar, Sunil Verma, M.S. Khan, K.S. Bartwal, Crystal Res. Technol. **44** (2009) 1303-1307.

[13] R.K. Choubey, P. Sen, P. K. Sen, R. Bhatt, S. Kar, K. S. Bartwal, Optical Mat. **28** (2006) 467-472.

[14] P. Sen, P. K. Sen, R. Bhatt, S. Kar, K. S. Bartwal, Solid State Commun. **129** (2004) 747-752.

[15] R.K. Choubey, B.Q. Khattak, S. Kar, P. Ramshankar, P. Sen, K.S. Bartwal, Crystal Research & Technol. **42** (2007) 718-722.

[16] R.V.A. Murthy, K.S. Bartwal, K. Lal, Mat. Sci. & Engg. B**18** (1993) L4-6.

[17] S. Kar, R.K. Choubey, P. Sen, G. Bhagavannarayana, K.S. Bartwal, Physica **B 393** (2007) 37-42.

[18] G. Bhagavannarayana, R.V.A. Murthy, G.C. Budakoti, B. Kumar, K.S. Bartwal, J. Appl. Crystallography, **38** (2005) 768-771.

[19] N. Kaithwas, S, Dave, S. Kar, S. Verma, K.S. Bartwal, Crys. Res. & Technol. **45** (2010) 1179-1182.

[20] S. Kar, Sunil Verma, K.S. Bartwal, J Alloys & Compd. **495** (2010) 288-291.

[21] R. Bhatt, S. Kar, K.S. Bartwal, V.K. Wadhawan, Solid State Commun. **127** (2003) 457-460.

[22] R.K. Choubey, R. Trivedi, M. Das, P. K. Sen, P. Sen, S. Kar, K.S. Bartwal, R. Ganeev, J. Crystal Growth, **311** (2009) 2597-2601.

[23] N. Sisodia, R. Trivedi, K.S. Bartwal, P. Sen, Nonlinear Opt. Quant. Opt. **39** (2009) 341-353.

[24] S. Kar, K.S. Bartwal, Crystal Growth & Design **7** (2007) 2522-2525.

[25] S. Kar, S. Verma, K.S. Bartwal, Crystal Research & Technology 43 (2008) 438-442.

[26] S. Kar, S. Verma, K.S Bartwal, Cryst. Res. & Technol. **44** (2009) 305-308.

[27] S. Kar, Sunil Verma, K. S. Bartwal, Physica B **405** (2010) 4299-4302.

We also observed that the torque exerted by LG trapping beam with high topological charges ($|l|$~ 15 or more) could drive RBCs as natural micro-rotors. For $|l|$ ~ 15 the trapped cells get aligned over the bright annulas of the LG trap due to larger circumference of the annulas. Under such condition the cells while being contained within the annular ring of light, orbits the beam axis in a direction determined by the handedness of the helical phase fronts. This is believed to be due to the transfer of light orbital angular momentum to the trapped cells by the scattering of the trap beam having helical wavefront. Figure T.3.7 shows the rotation of an RBC when trapped under l = 15 mode. The observed rotational frequency was ~ 12 rpm at ~ 15 mW of trapping power and it can be increased using higher trap beam power. To check whether the observed rotation is caused by the transferred light orbital angular momentum from the trap beam to the cell we changed the helicity of the trap beam. The sense of rotation was observed to get reversed as the charge of the LG mode was made negative. This allows for a means to change the sense of rotation of a micro-rotor system by simply changing the helicity of the trapping beam. A control on the sense of rotation can facilitate bi-directional operation for micro-machine components like micro-motors or valves.

(a) Minimization of photodamage in optical trap

Another area of concern while using optical tweezers for manipulation of biological cells, is the possibility of photoinduced adverse effects on the trapped cells. Because of the much reduced absorption by cells in the NIR spectral range (700–1100 nm), lasers operating in this spectral range are preferred for manipulation of cells. However, due to the large intensity (a few MW.cm^{-2} or higher) at the trap focus even with the use of lasers in the NIR spectral range, the possibility of adverse effects on the cells being manipulated is a matter of concern. Indeed adverse effects like a decrease in cloning efficiency and DNA damage have been reported in cells exposed to NIR optical trapping beam [21]. We have therefore explored the use of LG beams for manipulation of spermatozoa [22]. Due to its annular light profile, LG_{01} beam is known to have better trapping efficiency as confirmed with spherical particles. Further, LG modes have lower peak intensities compared to the usual Gaussian mode for identical beam power. We realized that these properties of LG beams can offer important advantage for manipulating biological cells by reducing the level of photodamage. Since nowadays spermatozoa are being routinely manipulated by laser tweezers for assessing quality of sperm samples and assisting the *in vitro* fertilization method, we chose spermatozoa as the model biological cells. The results of our studies revealed two important advantages: firstly, LG_{01} mode offers better trapping efficiency than TEM_{00} mode for highly motile spermatozoa and second, the light damage on the cells is significantly reduced with LG beams.

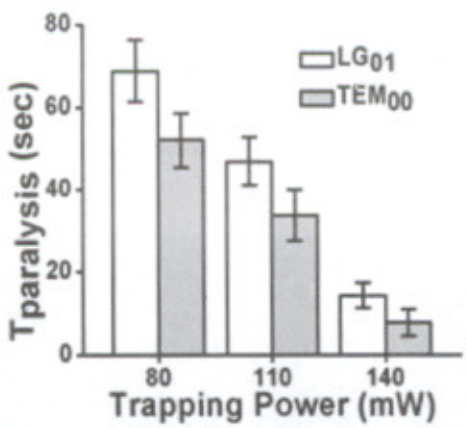

Fig.T.3.8: One $T_{paralysis}$ of the trapped spaermatozoa under TEM_{00} and LG_{01} mode. The data presented are the mean ± standard deviation.

Since it was observed that after getting trapped the strong flagellar motion of the cells gradually decays and finally stops after a time period ($T_{paralysis}$) characteristic of the adverse effects of the trapping beam onto the cells, in Fig T.3.8 the change in $T_{paralysis}$ of the trapped spermatozoa under different trapping modes are shown. The reason for reduced light damage on the cells by LG modes is believed to be due to lowered degree of nonlinear absorption of trapping light and experiments performed with acridine orange stained cells supported this conjecture. Considering high level of concern over the genetic purity of spermatozoa the results should motivate evaluation of the special laser beams for manipulating the cells.

(a) Raman spectroscopy of optically trapped RBCs

Raman optical tweezers are being extensively used for studying RBCs since Raman spectroscopy is a powerful technique to monitor the oxygen carrying capacity of RBCs because the binding or the dissociation of oxygen with heme leads to significant conformational changes of hemoglobin that can be sensitively monitored by this technique. We used the Raman tweezers set-up for studying the spectra from RBCs taken from patients suffering from malaria (*Plasmodium vivax* infection). In Figure T.3.9 we show the mean Raman spectrum of RBCs collected from blood samples of five healthy volunteers. Spectra from at least 15 RBCs were recorded from each sample. The mean spectrum